The protein tyrosine phosphatase RPTPζ/phosphacan is critical for perineuronal net structure

Received for publication, August 27, 2019, and in revised form, December 9, 2019 Published, Papers in Press, December 10, 2019, DOI 10.1074/jbc.RA119.010830

Geoffrey J. Eill[‡1], Ashis Sinha[‡1], Markus Morawski[§], Mariano S. Viapiano[‡¶], and Russell T. Matthews[‡]

From the [‡]Department of Neuroscience and Physiology and [¶]Department of Neurosurgery, State University of New York Upstate Medical University, Syracuse, New York 13210 and [§]Paul Flechsig Institute of Brain Research, University of Leipzig, Jahnallee 59, D-04109 Leipzig, Germany

Edited by Gerald W. Hart

Perineuronal nets (PNNs) are conspicuous neuron-specific substructures within the extracellular matrix of the central nervous system that have generated an explosion of interest over the last decade. These reticulated structures appear to surround synapses on the cell bodies of a subset of the neurons in the central nervous system and play key roles in both developmental and adult-brain plasticity. Despite the interest in these structures and compelling demonstrations of their importance in regulating plasticity, their precise functional mechanisms remain elusive. The limited mechanistic understanding of PNNs is primarily because of an incomplete knowledge of their molecular composition and structure and a failure to identify PNN-specific targets. Thus, it has been challenging to precisely manipulate PNNs to rigorously investigate their function. Here, using mouse models and neuronal cultures, we demonstrate a role of receptor protein tyrosine phosphatase zeta (RPTPζ) in PNN structure. We found that in the absence of RPTPζ, the reticular structure of PNNs is lost and phenocopies the PNN structural abnormalities observed in tenascin-R knockout brains. Furthermore, we biochemically analyzed the contribution of RPTPζ to PNN formation and structure, which enabled us to generate a more detailed model for PNNs. We provide evidence for two distinct kinds of interactions of PNN components with the neuronal surface, one dependent on RPTPζ and the other requiring the glycosaminoglycan hyaluronan. We propose that these findings offer important insight into PNN structure and lay important groundwork for future strategies to specifically disrupt PNNs to precisely dissect their function.

Studies over the past two decades have identified the important and perhaps fundamental role for the neural extracellular matrix (ECM)[3] in regulating neuronal plasticity in the central nervous system (CNS). For example, manipulation of the neural ECM disrupts developmental ocular dominance plasticity in the primary visual cortex and modulates learning and memory in multiple regions within the brain (1–3). Indeed, alterations and/or disruptions of the neural ECM are associated with a number of neuropsychiatric disorders and neurodegenerative diseases (4–8). Importantly, these studies primarily attribute these functions to a unique and enigmatic neural ECM substructure called the perineuronal net (PNN).

PNNs are conspicuous reticular ECM formations that ensheathe limited but specific subsets of neurons in the CNS (9, 10). These highly aggregated ECM structures surround the cell body and proximal neurites of ensheathed neurons but appear to be excluded from sites of synaptic contact thereby giving them a lattice-like or net-like appearance. Early work noted that expression of PNNs in primary sensory cortices, such as visual and somatosensory cortex, is activity dependent and that the timing of their appearance is consistent with closure of developmental critical periods such as the critical period for ocular dominance plasticity (11, 12). Furthermore, in the cortex, PNNs are particularly enriched surrounding parvalbumin-expressing interneurons, which are known to be key regulators of developmental plasticity. Therefore, it is hypothesized that PNNs may be important regulators of developmental plasticity in the developing cortex.

Previous work showed that PNNs are particularly enriched in the glycosaminoglycan hyaluronan (HA) and hyaluronan-binding chondroitin sulfate proteoglycans (CSPGs). The presence of highly aggregated CSPGs in PNNs has received particular attention because CSPGs are notoriously inhibitory molecules in the CNS and a major barrier to regeneration in the injured nervous system (13–15). Therefore, the appearance of CSPG-enriched structure surrounding synapses coincident with closure of the period of heightened developmental plasticity led to the hypothesis that these structures likely inhibit synaptic plasticity. Consistent with this hypothesis more recent studies demonstrated that, indeed, disruption of the neural ECM and PNNs in the visual cortex restores juvenile ocular dominance

This work was supported by NINDS, National Institutes of Health Grant NS069660 (to R. T. M.) and by the German Research Foundation (DFG) Priority Program 1608 "Ultrafast and temporally precise information processing: Normal and dysfunctional hearing" Mo2249/2–1, Mo2249/2–2 (to M. M.) and the Alzheimer-Forschung-Inititiative (AFI) 18072 (to M. M.). The authors declare that they have no conflicts of interest with the contents of this article. The content is solely the responsibility of the authors and does not necessarily represent the official views of the National Institutes of Health.

This article contains Fig. S1.

[1] These authors contributed equally to this work and are listed alphabetically.

[2] To whom correspondence should be addressed: 750 East Adams St., Syracuse, NY 13210. Tel.: 315-464-7766; Fax: 315-464-7727; E-mail: matthewr@upstate.edu.

[3] The abbreviations used are: ECM, extracellular matrix; CNS, central nervous system; PNN, perineuronal net; HA, hyaluronan; CSPG, chondroitin sulfate proteoglycan; ChABC, chondroitinase ABC; RPTPζ, receptor protein tyrosine phosphatase zeta; IHC, immunohistochemistry; WFA, *Wisteria floribunda* agglutinin; PFA, paraformaldehyde; ANOVA, analysis of variance; DIV, day *in vitro*; PND, postnatal day; E, embryonic day; Tnr, tenascin-R.

plasticity in mature rodent brain (1). Importantly these findings suggest that ECM and PNN disruption alone is sufficient to reopen juvenile plasticity, indicating that these are critical regulators of neural plasticity.

The body of work linking PNNs to developmental plasticity (16–18) is quite compelling, however; an ever-growing list of studies now links PNNs to a vast array of neural functions and pathologies. Of particular interest are prominent roles for PNNs in other forms of plasticity such as learning and memory. An explosion of recent work demonstrated that manipulating the ECM and PNNs in multiple brain regions including the amygdala, hippocampus, cortex, and striatum significantly alters learning and memory (2, 3, 19–22). Although these results are quite striking and exciting for the field, a mechanistic understanding of PNN function has been surprisingly elusive. We still do not understand what the precise function of PNNs is nor how they modulate plasticity. In addition, there are conflicting findings from different labs with PNN manipulations that further highlight the limits of our understanding of this structure (23, 24).

The limited mechanistic understanding of PNN function is derived primarily from an incomplete understanding of its molecular composition and structure and, in turn, the inability to specifically disrupt PNNs without disrupting the surrounding ECM. For example, much of the work identifying roles for PNNs in various forms of plasticity has relied on enzymatic digestion with chondroitinase ABC (ChABC). This treatment impacts PNNs but does not necessarily eliminate the structure, and even disrupts the surrounding ECM (25). Additionally, genetic models disrupting specific PNN components have provided insight into their function, but also typically impact the surrounding neural ECM. Therefore, the goal of this study is to provide a more complete understanding of PNN structure toward the ultimate goal of developing more precise strategies to specifically disrupt PNNs to better study their function.

In this study we detail a novel role for receptor protein tyrosine phosphatase zeta (RPTPζ) in the structure of PNNs. Utilizing mouse models and neuronal cultures, we demonstrate RPTPζ is critical for the proper formation of PNNs. Further analysis using molecular and biochemical techniques shows PNNs are bound to the neuronal surface through two distinct mechanisms, one requiring hyaluronan and the other RPTPζ. Overall, our data provide novel insights into the structure and formation of PNNs to ultimately develop tools to precisely determine PNN function.

Results

PNNs are disrupted in Ptprz1 KO adult mice

A detailed understanding of PNN function has been elusive due in large part to an incomplete understanding of their composition and structure. In this regard the role of RPTPζ in PNNs is intriguing because although it has been localized to PNNs, its role in these structures has never been thoroughly studied. Although virtually all other proteins identified in PNNs are secreted proteins, the full-length isoform of RPTPζ is a large transmembrane protein and thereby could provide a key anchor point for PNNs to the neuronal cell surface. Furthermore, RPTPζ is a phosphatase and could also serve a signaling function in PNNs. Finally, RPTPζ is known to interact with other key PNN components such as Tnr and could provide a key link to the other components in this structure. Therefore, we investigated PNN structure in *Ptprz1* KO mice. Of note, the nomenclature surrounding the protein products of the *Ptprz1* gene, RPTPζ and phosphacan, in the literature is somewhat confusing. This largely stems from various laboratories isolating the proteoglycan using different monoclonal antibodies. As such RPTPζ is also known by DSD-1, 6B4, 3F8, and RPTPβ. It is now generally accepted that the receptor form be described as RPTPζ, to match its gene *Ptprζ1* (*Ptprz1*). Therefore, in this article, we will designate all protein isoforms of the *Ptprz1* gene as RPTPζ and specifically name the secreted variant phosphacan where relevant.

Before investigating PNN structure, we confirmed the loss of RPTPζ of our *Ptprz1* KO mice through immunostaining using RPTPζ-specific antibody 3F8 in adult cortical sections (Fig. S1*A*). 3F8 staining was essentially eliminated in the brains of the knockout animals confirming the validity of this model. We subsequently immunostained cortical sections of PND 90 brains with the most well-established markers of PNNs, antibodies directed against aggrecan and the lectin WFA. In WT brains, PNNs had the typical highly organized lattice structure on a subset of neurons in the cortex. However, PNNs in the KO brains appeared altered in structure and less organized than their WT counterparts. Upon closer observation, we noted that although typical PNN staining reveals bridgelike strings interconnecting foci along the neuronal surface that create discrete gaps or holes that give a netlike appearance, these "bridges" seemed largely absent in the KO brains (Fig. 1). Interestingly PNNs in brains from heterozygous mice seemed largely unaffected. In the KO animals, however, instead of the intricate, lattice-like structure as seen in WT, PNN components aggregated on the neuronal surface, creating prominent foci. Despite this disrupted structure, interestingly, PNN areal and cell-specific distribution remained unaffected in *Ptprz1* KO mice. In addition, we found this disruption occurred as early as PND 21 (Fig. S1*B*). From these data, we concluded RPTPζ is necessary for proper formation of PNNs from early in mammalian development through maturity.

To quantify the disrupted PNN phenotype, we analyzed two aspects of PNN staining: PNN intensity and PNN spatial distribution on the neuronal surface. Cortical brain slices were stained with WFA and individual PNN-bearing neurons were imaged and analyzed across the *Ptprz1* brains (WT, $n = 4$ animals, 55 PNNs; Het, $n = 3$ animals, 26 PNNs; KO, $n = 4$ animals, 43 PNNs). From our initial observations, we found that disrupted *Ptprz1* KO PNNs had large areas devoid of PNN staining, possibly because of component aggregation and collapse of the stringlike interconnections (Fig. 2*A*). To quantify this observation, we first developed a binary gap analysis as described in "Experimental procedures" (Fig. 2). A binary process converts any image of varying pixel intensity to black and white using a unbiased calculated threshold, making it a useful analysis tool to assess the empty space of an image (Fig. 2*B*). Of particular interest, the binary image of control PNNs distinctly shows the well-defined gaps and regular lattice-like structure of

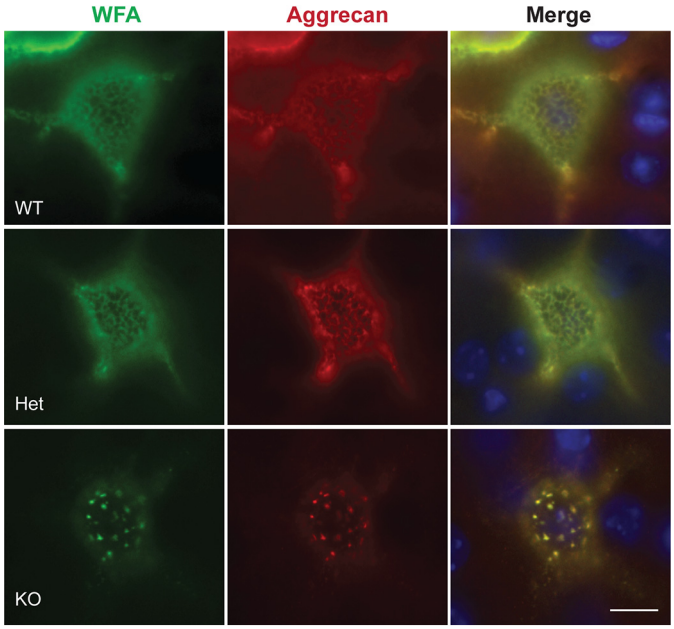

Figure 1. Perineuronal nets are disrupted in *Ptprz1* KO adult mice. Cortical sections from PND 90 adult *Ptprz1* KO and WT mice were stained with antibodies against aggrecan and the lectin WFA (*Wisteria floribunda* agglutinin) to detect PNNs. In littermate WT and Het, typical lattice-like PNN structures were observed. In addition, there were no discernable differences in structure between the two genotypes. However, PNNs in sections from *Ptprz1* KO mice the lattice-like PNN structure is lost with aggrecan and subsequently WFA staining appearing aggregated on the neuronal surface. *Scale bar*, 10 μm.

PNNs. In *Ptprz1* KO mice, however, the gaps are no longer well-defined and PNN staining appears aggregated and discontinuous leading to gaps or large areas of no PNN staining. After calculating the black/white pixel count ratio, we found no significant difference between *Ptprz1* WT and Het PNNs (data not shown), therefore the data sets were combined. In *Ptprz1* KO PNNs, however, we found a significantly higher black/white pixel count ratio ($p = 1.09 \times 10^{-5}$, Student's *t* test), confirming greater areas of no PNN staining (Fig. 2*C*).

The above method effectively describes the ratio of PNN-containing regions to regions devoid of PNN staining on the surface of neurons between *Ptprz1* WT/Het and *Ptprz1* KO animals. However, in addition to this, PNN staining from the *Ptprz1* KO neurons appears discontinuous and aggregated in contrast to the more regular, continuous staining seen in *Ptprz1* WT/Het animals. To quantify this element of PNN structure we developed a PNN peak or node analysis. This method takes into account the difference in spatial distribution and clustering of PNN staining on the cell surface between the different groups. As before we utilized WFA as a marker for PNNs. We determined the sharpness of PNN peaks seen on the neuronal surface using the local maxima function in ImageJ (Fig. 2, *D* and *E*). The more continuous and regular WFA staining of the *Ptprz1* WT/Het group resulted in significantly higher number of nodes or peaks in this genotype. The aggregated staining of the *Ptprz1* KO PNNs led to detection of significantly fewer nodes ($p = 0.0009$, Student's *t* test), which also appeared more isolated than in *Ptprz1* WT/Het animals (Fig. 2*F*). The average prominence of PNN nodes over their surrounding space in the *Ptprz1 KO* PNNs was also significantly higher compared with *Ptprz1* WT/Het PNNs ($p = 0.014$, Student's *t* test) (Fig. 2*G*). Both these data indicate the regular continuous structure of PNNs in the *Ptprz1* WT/Het animals and the broken discontinuous PNN staining seen in *Ptprz1* KO cells. The increase in the average prominence levels of WFA peaks in the *Ptprz1* KO PNNs further points to the isolated nature of PNN nodes and the loss of connections between them in the *Ptprz1* KO animals.

ECM components remain bound to disrupted PNN structures in Ptprz1 KO mice

Although our data indicate that proper PNN structure is disrupted in *Ptprz1* KO mice, the impact of RPTPζ on the other known PNN components remains unclear. To further define how RPTPζ contributes to the underlying structure of PNNs, we stained cortical sections of adult *Ptprz1* mice with PNN markers WFA, aggrecan, HAPLN1, neurocan, brevican, and Tnr, and further quantified for fluorescent intensity (Fig. 3, *A*). Although staining with all components showed the same aggregate PNN structure found with aggrecan and WFA, all ECM components, including Tnr, remained bound to PNNs in *Ptprz1* KO mice. Quantifying the various PNN components, and accounting for sex, we found no significant ECM intensity difference between *Ptprz1* WT ($n = 9$; 3 males, 6 females) and *Ptprz1* Het ($n = 12$; 6 males and 6 females) mice for most of the PNN components. When compared with *Ptprz1* KO mice ($n = 14$; 4 males, 10 females), we only found significant losses in WFA ($p = 6.53 \times 10^{-5}$, Student's *t* test) and aggrecan ($p = 0.01$) whereas no significant losses were seen for all other PNN components analyzed.

Expression of aggrecan and hyaluronic and proteoglycan link protein 1 (HAPLN1) in the cortex of *Ptprz1* mice was analyzed via Western blot analysis ($n = 3$ per genotype) (Fig. 3*B*). Similar to IHC results, aggrecan protein levels in the cortex were significantly reduced in *Ptprz1* KO mice ($p = 0.03$, Student's *t* test), while HAPLN1 protein levels remained unchanged ($p = 0.64$). To ensure aggrecan loss did not occur at the transcription level, we performed an RT-PCR analysis and found no significant changes in gene expression across all *Ptprz1* (data not shown). From these analyses, we conclude that although important for proper structural formation, the loss of RPTPζ does not affect the overall localization of ECM components to the PNN surface.

The PNN disruption in Ptprz1 KO mice phenocopies the PNN disruption in tenascin-R KO mice

We next sought to determine a mechanism in which RPTPζ anchors PNNs to the surface. We noted that the PNN phenotype we observed in the *Ptprz1* KO brains looked remarkably similar to the phenotype found previously in *Tnr* KO brains (26, 27). Additionally, Tnr is of particular interest because it is a high-affinity binding partner of RPTPζ (28–30). To confirm our observations, we obtained PFA-fixed PND 90 adult brains of *Tnr* WT and *Tnr* KO mice and directly compared the PNN phenotype to *Ptprz1* KO mice (Fig. 4). Staining with WFA and aggrecan antibody, PNNs in *Tnr* WT resembled a typical lattice-like structure as observed with *Ptprz1* WT/Het PNNs. The lattice-like structure of controls was completely absent and replaced by areas of aggregation. More importantly, these phe-

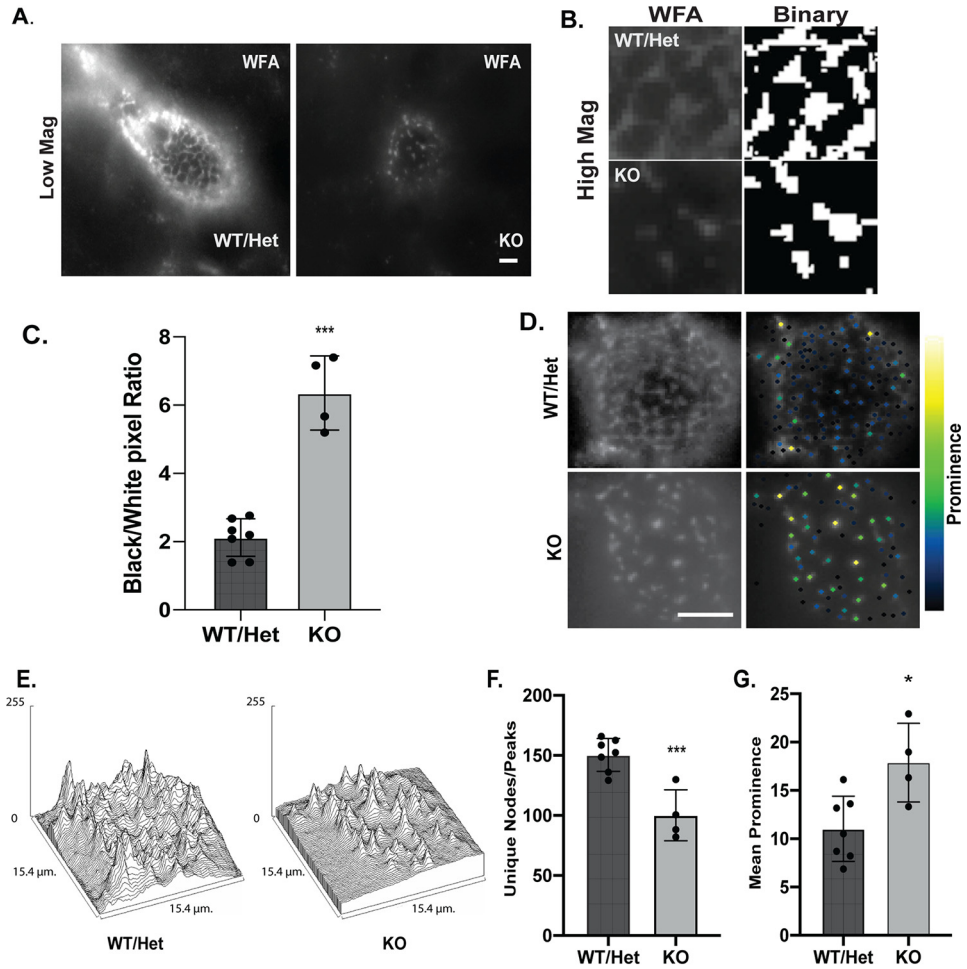

Figure 2. PNNs from *Ptprz1* WT or *Ptprz1* Het mice are distinct from those derived from *Ptprz1* KO animals. PNNs from PND 90 adult WT, Het, and KO mice were stained with WFA and quantified. WT and Het animals showed no statistically significant difference in any of the following analyses and were grouped together as WT/Het. *A*, PNNs from WT/Het appear brighter and show regular meshlike PNN appearance whereas KO PNNs show decreased WFA intensity and a disrupted staining pattern. *B*, shows a magnified view of the surface of the cells in A converted to binary images. *C*, KO animals showed significantly higher black/white pixel ratio, indicating an increased area devoid of PNN staining ($p = 1.09 \times 10^{-5}$, two-tail Student's *t* test, S.D. for *error bars*). *D*, representative image of WT/Het and KO PNNs for PNN node/peak analysis at varying prominence levels. *Yellow* color dots represent nodes/peaks of highest prominence (more isolated) followed by *green*, *blue*, and *black*. *E*, representative surface intensity profile of PNNs from WT/Het and KO animals. WT/Het PNNs show greater number of peaks as compared with KO PNNs. KO PNNs also appear more isolated with sharper peaks. *F*, WT/Het PNNs showed significantly higher number of peaks as compared with *Ptprz1* KO PNNs ($p = 0.0009$, two-tailed Student's *t* test, S.D. for *error bars*).*G*, the average isolation index of PNN peaks (represented here as the mean prominence level of all the peaks) was significantly higher in KO PNNs as compared with WT/Het PNNs ($p = 0.014$, two-tailed Student's *t* test, S.D. for *error bars*) indicating the fewer and more sharp peaks in case of the KO animals. Binary image analysis and PNN peak/node analysis were carried out on WT ($n = 4$ animals, 55 PNNs), Het ($n = 3$ animals, 26 PNNs), KO ($n = 4$ animals, 43 PNNs). Images in (*B*) are 5 μm $\times$ 5 μm. *Scale bar*, 5 μm.

notypes were indistinguishable from PNNs in *Ptprz1* KO mice. From these data, we concluded RPTPζ likely interacts with Tnr to mediate PNN structure.

PNN component aggrecan is immobilized on the cell surface by a distinct HA- and EDTA-sensitive interaction

Previous work has identified and demonstrated the importance of Tnr, HAPLN1, and the lectican CSPGs, aggrecan, neurocan, and brevican, in the proper formation of PNNs (23, 26, 27, 30–41). We have found PNNs to be disrupted in *Ptprz1* KO mice. However, the exact mechanism by which these components bind together to form PNNs is not clear. To better understand the mechanism of binding of PNN components we established a biochemical release assay to measure binding of aggrecan to the neuronal cell surface. Aggrecan is the best PNN component for this analysis because it is the most PNN-specific component and recently has been shown to be perhaps the key CSPG in PNN formation (24). Our finding of the potential interaction between RPTPζ and Tnr in PNN structure led to our hypothesis that we should be able to disrupt this element of PNN structure by chelating calcium. The interaction between RPTPζ and Tnr is Ca^{2+} dependent and, subsequently, the interaction of Tnr with aggrecan also depends on Ca^{2+}. Therefore, we reasoned that treatment with EDTA would disrupt this entire complex and if this complex were involved in PNN cell-surface binding, would enhance the release of aggrecan. In addition, current models of PNN structure suggest that aggrecan is immobilized to the cell surface by interacting with the PNN backbone made up of the glycosaminoglycan HA (32, 40, 42). Therefore, we reasoned digestion of HA should also increase the release of aggrecan. If both mechanisms are independently involved in the binding of aggrecan to the neuronal membrane then we hypothesized that in the *Ptprz1* and *Tnr* KO brain, aggrecan release would depend only on HA. To test this

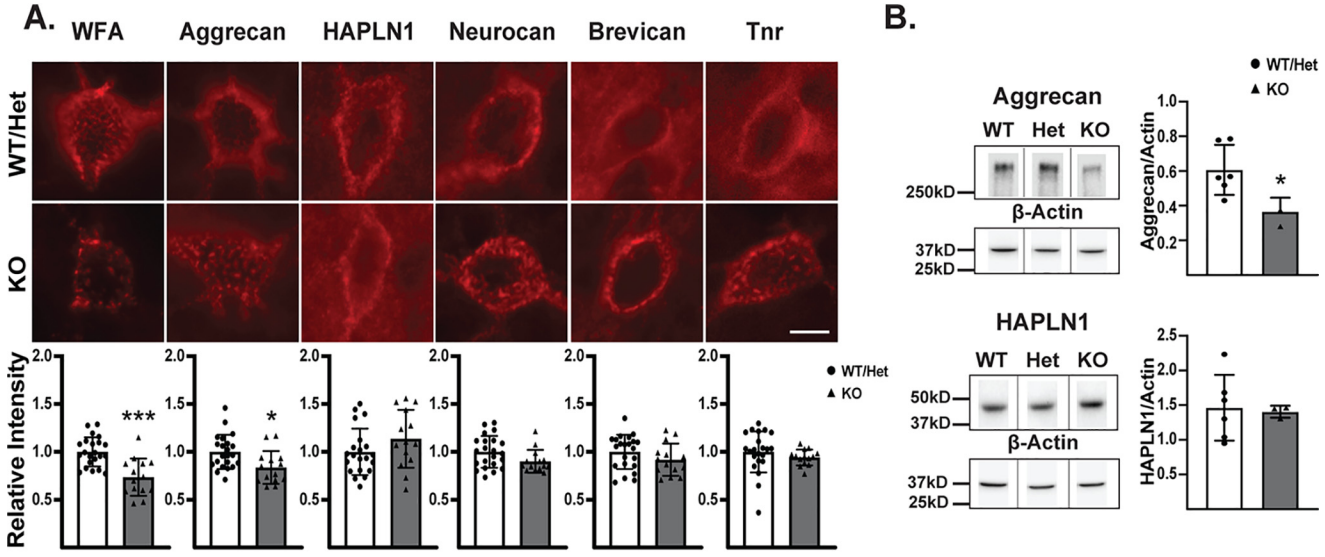

Figure 3. PNN component analysis of the *Ptprz1* KO and WT mice. *A*, to understand the role of RPTPζ on PNN components, cortical sections of PND 90 adult *Ptprz1* KO and WT mice were stained with markers WFA, aggrecan, HAPLN1, neurocan, brevican, and Tnr. Despite following the disrupted structure shown with WFA and aggrecan, ECM components remain bound to PNNs in the *Ptprz1* KO. PNN component IHC intensities were quantified (as described in the "Experimental procedures" section), showing a significant loss of only WFA ($p = 6.53 \times 10^{-5}$) and aggrecan ($p = 0.01$) in *Ptprz1* KO mice (KO, $n = 14$ animals; WT/Het, $n = 21$ animals), whereas there were no significant differences with other PNN markers. *Scale bar*, 10 μm. *B*, to confirm partial loss of specific PNN components, we analyzed aggrecan and HAPLN1 protein expression, via Western blotting, from the cortex of *Ptprz1* KO and WT mice ($n = 3$ per genotype, no significant differences between WT and Het). In the PND 90 adult cortex, aggrecan protein was significantly decreased in *Ptprz1* KO ($p = 0.03$), whereas there were no significant differences in HAPLN1expression ($p = 0.64$, Student's *t* test, S.D. for *error bars*).

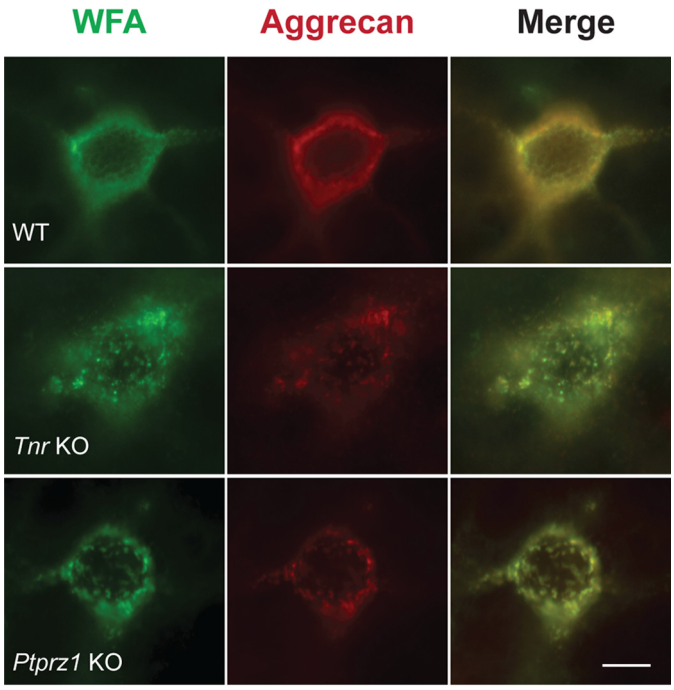

Figure 4. PNN disruption in *Ptprz1* KO mice phenocopies the PNN disruption in *Tnr* KO mice. *Tnr* knockout is known to disrupt PNN structure and is a well-known binding partner of RPTPζ. We hypothesized the PNN phenotype in *Ptprz1* KO mice might be a phenocopy of PNN structure in *Tnr* KO mice. Staining with PNN markers aggrecan and WFA on WT PND 90 cortices showed a typical lattice-like PNN structure. However, PNNs in *Ptprz1* KO showed identical aggregated PNN structures to *Tnr* KO mice. *Scale bar*, 10 μm.

hypothesis, we isolated membranes from adult mouse brains and assessed the release of aggrecan by HA digestion in WT, *Ptprz1* KO, and *Tnr* KO tissue (Fig. 5). We found that there is very little release of aggrecan from brains of WT mice (15 ± 9%). In contrast, there was significant difference in release of aggrecan among the groups (one-way ANOVA $F(2,7) = 14.94$, $p = 0.003$). Both *Ptprz1* KO brains (42 ± 4%, $p = 0.0340$) and *Tnr* KO brains (58 ± 13%, $p = 0.0024$) showed greater release as compared with WT. Interestingly, the vast majority of aggrecan was released from WT brains in our ChABC in conjunction with EDTA treatment assays (82 ± 7%). *Ptprz1* KO brains (87 ± 19%) and *Tnr* KO (80 ± 27%) brains also showed an increase and similar levels of aggrecan release to WT brains when treated with both ChABC and EDTA.

These data indicate that in WT mice aggrecan is immobilized on the cell surface by a dual interaction which is sensitive to HA digestion and EDTA, respectively. Attachment of aggrecan in either *Ptprz1* KO or *Tnr* KO brains is compromised and the EDTA-sensitive mechanism of aggrecan binding is lost. These data along with the fact that aggrecan is similarly solubilized in our biochemical release assay from *Ptprz1* KO and *Tnr* KO brains suggest that these two proteins are involved in aggregating this CSPG to the cell surface via the same mechanism. We next proceeded to further test the role of RPTPζ and Tnr in immobilizing aggrecan to the cell surface.

Tnr and RPTPζ are both required to bind aggrecan to the cell surface

The role of Tnr in proper formation of PNNs is well-known and has been demonstrated in a number of systems, including brain slices, organotypic cultures, and dissociated neurons from *Tnr* KO mice (26, 37, 38). Here we show RPTPζ disruption phenocopies the PNN structural deficit found in the *Tnr* KOs. Because RPTPζ and Tnr are high-affinity ligands for each other, we hypothesize these proteins interact in mediating PNN structure. To more thoroughly characterize the binding of aggrecan to the cell surface through RPTPζ and Tnr, we endeavored to recapitulate the effect in HEK293 cells, a cell line that does not

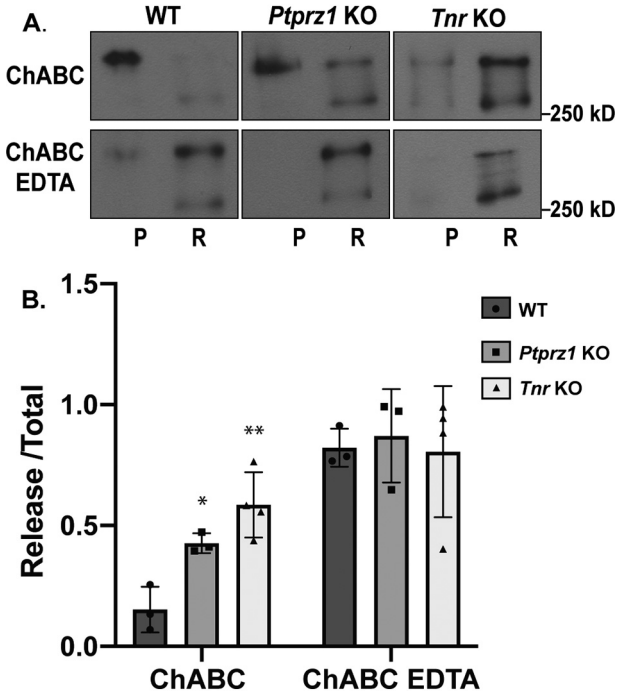

Figure 5. Membrane binding of the key PNN component aggrecan is biochemically altered in *Ptprz1* KO and *Tnr* KO mice brains. Brain homogenates were treated with ChABC to remove the hyaluronan backbone of PNNs or chondroitinase in the presence of EDTA (ChABC EDTA) and centrifuged to obtain soluble release (*R*) and insoluble pellet (*P*) fractions. *A*, Western blotting image showing release of PNN marker aggrecan into soluble phase from brain homogenates of WT, *Ptprz1* KO, and *Tnr* KO mice by ChABC treatment alone and ChABC EDTA treatment. The release of aggrecan into the soluble fraction required ChABC treatment in addition with EDTA in WT brain homogenates. Aggrecan was released more readily with just ChABC treatment in *Ptprz1* KO and *Tnr* KO animals. *B*, quantification showing ratio of the soluble release fraction (*R*) to total aggrecan levels (soluble release (R) + insoluble pellet (P)) in WT, *Ptprz1* KO, and *Tnr* KO mice. There was a statistically significant difference in the release of aggrecan among the three genotypes as determined by one-way ANOVA ($F(2,7) = 14.94$, $p = 0.0030$). A Tukey's post hoc test showed that aggrecan was released much more readily in *Ptprz1* KO mice ($42 \pm 0.04\%$, $p = 0.0340$) as well as in *Tnr* KO mice ($58 \pm 13\%$, $p = 0.0024$) compared with WT mice ($15 \pm 9\%$) when treated with just ChABC. There was no significant difference in aggrecan release between *Ptprz1* KO and *Tnr* KO brains. Treatment with ChABC alongside EDTA led to almost complete release of aggrecan into the soluble release fraction in all genotypes. The ratio of release to total in *Ptprz1* KO, *Tnr* KO and WT mice was not significantly different among the genotypes in the ChABC with EDTA treatment group. *B*, *bars* in graphs represent percentage release ± S.D.

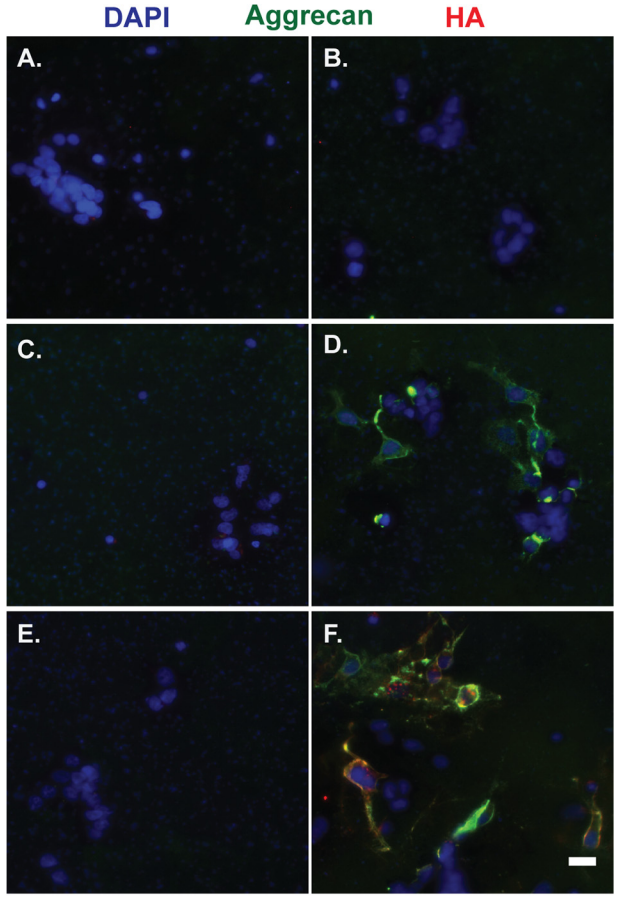

Figure 6. RPTPζ and Tnr are both required for binding aggrecan to the cell surface and binding of aggrecan is enhanced by presence of HA. Exogenous aggrecan was added to HEK293 cells in the presence of Tnr and/or RPTPζ. HA was expressed in the system and the cells were fixed and stained to detect bound aggrecan on the cell surface. *A*, HEK293 cells do not express PNN component aggrecan on their own. *B*, adding aggrecan exogenously to HEK293 cells does not lead to binding on the cell surface. *C*, adding aggrecan and Tnr does not lead to binding of aggrecan. *D*, aggrecan binds to the cell surface when both RPTPζ and Tnr are present. *E*, presence of RPTPζ alone is not able to bind aggrecan to the cell surface. *F*, expressing HA in (*D*) *i.e.* in presence of both RPTPζ and Tnr enhances binding of aggrecan. These data indicate that the binding of aggrecan to the cell surface depends on both RPTPζ and Tnr and binding is enhanced in the presence of HA. *Scale bar*, 10 μm.

form PNNs endogenously (Fig. 6). We found that adding aggrecan alone or aggrecan and Tnr does not result in binding the CSPG to the cell (Fig. 6, *A–C*). This is not completely surprising as Tnr is a secreted glycoprotein and does not contain any transmembrane domains to anchor it to the cell surface. Thus, its primary role is likely involved in the crosslinking PNN components but does not immobilize them on the cell. We then tested whether the binding of Tnr to the cell surface can be mediated by RPTPζ by expressing a construct containing the Tnr binding domain of RPTPζ in the HEK293 cells (Fig. 6, *D–F*). We found that in the presence of Tnr, cells expressing RPTPζ formed pericellular aggregates of aggrecan (Fig. 6*D*). Furthermore, HEK293 cells did not bind aggrecan when only RPTPζ was expressed, but required the presence of Tnr. These results demonstrate that both these two proteins are required to bind aggrecan to the cell surface. Interestingly, adding HA to these cells further enhanced staining and the netlike appearance of the structure highlighting the importance of HA in the aggregating PNN components to the cell surface (Fig. 6*F*).

Ptprz1 KO neurons show disrupted PNN distribution and distinct biochemical properties in culture as compared with WT neurons

Dissociated neuronal cultures present an attractive model to study binding of PNN components to the neuronal surface. This model system allowed us to perform biochemical analysis in live cells. We therefore utilized dissociated neuronal cultures to more thoroughly assess the role of RPTPζ in binding PNN components to the cell surface. Cultures were derived from E16 CD1 WT and *Ptprz1* KO mice and were positive for PNN marker aggrecan (Fig. 7, *A* and *E*). However, staining in the *Ptprz1* KO cells appeared disrupted and reduced in intensity as compared with the WT cultures, indicating the role of RPTPζ

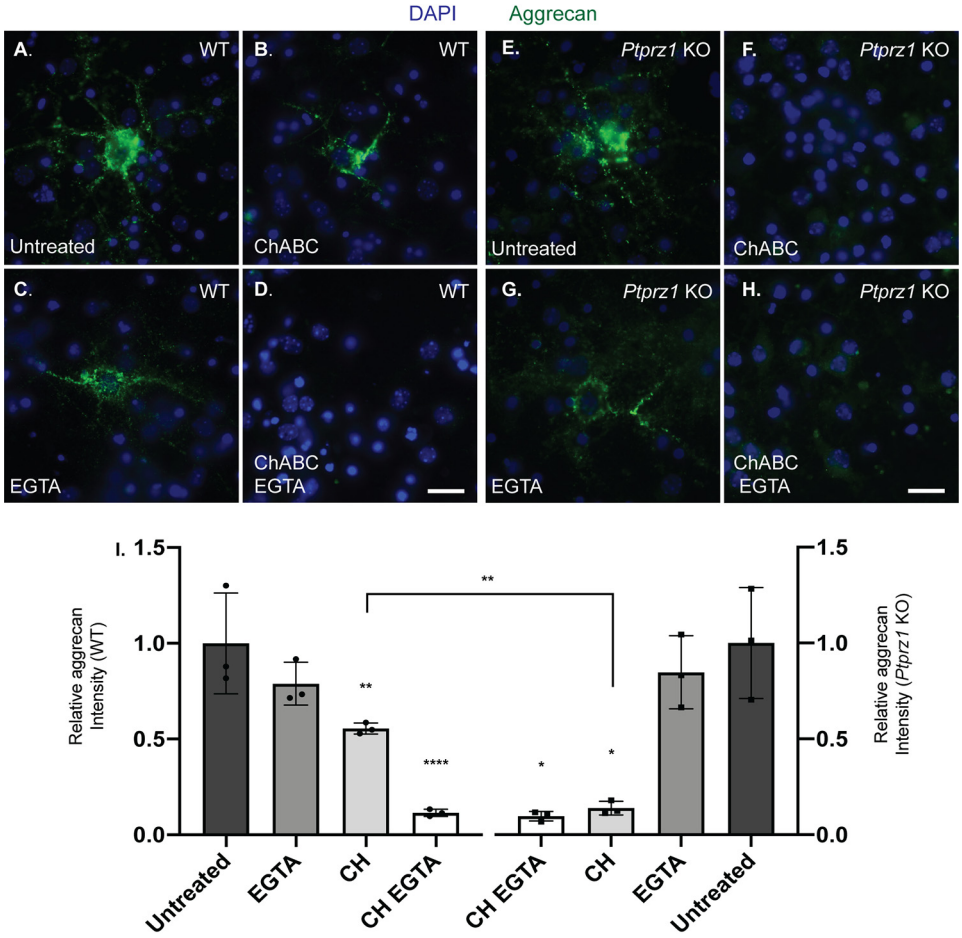

Figure 7. Digestion of HA is sufficient to eliminate staining for PNN component, aggrecan in *Ptprz1* KO neurons. Neurons derived from E16 WT and *Ptprz1* KO mice were treated with ChABC to digest HA and/or EGTA to chelate calcium. Both WT as well as *Ptprz1* KO neurons were positive for aggrecan at 9 DIV (*A* and *E*). Digesting away the HA backbone of PNNs lead to a relatively minor reduction of aggrecan staining in the WT cultures (*B*). However, in contrast, *Ptprz1* KO cultures with HA digestion showed a dramatic reduction in aggrecan staining (*F*). Acute treatment with EGTA alone resulted in only a minor loss of aggrecan staining in both the genotypes (*C* and *G*). A combination of the above treatments *i.e.* digesting away HA in conjunction with EGTA treatment resulted in virtually a complete loss of PNN component staining in both WT and *Ptprz1* KO cultures (*D* and *H*). To quantify these findings, the ratio of aggrecan intensity was calculated for WT and *Ptprz1* KO cultures and is presented here in a graphical form (*I*). Analysis by two-way ANOVA showed significant differences by genotype ($F(1,16) = 69.57$, $p < 0.0001$), treatment ($F(3,16) = 36.46$, $p < 0.0001$), and interaction between the two ($F(3,16) = 5.479$, $p = 0.0088$). Most importantly although Tukey's post hoc test showed significant loss of aggrecan staining with ChABC alone in both WT and KO cells ($p = 0.0042$ and $p = 0.0202$, respectively), there was significantly more loss in the KO cells compared with WT cells ($p = 0.0015$). A combination of ChABC and EGTA treatment resulted in a significant loss of aggrecan in both genotypes as compared with their respective untreated conditions (WT $p < 0.0001$, *Ptprz1* KO $p = 0.0137$) but no significant differences between genotypes. EGTA alone had no significant effect of aggrecan staining. These findings indicate that in WT cells PNN components are attached to the cell surface by two mechanisms, being HA dependent and calcium sensitive, respectively. These interactions are compromised in *Ptprz1* KO cultures, and PNN components are immobilized on the neuronal surface only in a HA-dependent manner. *Bars* in graphs represent relative aggrecan intensity to untreated condition of the corresponding genotype ± S.D. (*B*). *Scale bar*, 10 μm.

in binding PNN components to the cell surface. Our previous findings have shown that the interaction of aggrecan with the cell surface is mediated by RPTPζ and Tnr. Further, this interaction depends on two kinds of mechanisms, being sensitive to HA digestion and Ca^{2+} ions, respectively. To determine the binding mechanism of aggrecan to cell surface and the role of RPTPζ in PNN formation we treated neuronal cultures from WT and *Ptprz1* KO mice acutely with ChABC and/or EGTA. There are significant effects of genotype ($F(1,16) = 69.57$, $p <$ 0.0001) and treatment ($F(3,16) = 36.46$, $p < 0.0001$) as well as interaction ($F(3,16) = 5.479$, $p = 0.0088$) on aggrecan staining when analyzed by two-way ANOVA. Tukey's post hoc testing (Fig. 7*I*) showed that acute treatment with ChABC alone had only a moderate effect on the release of aggrecan from WT cultures (Fig. 7*B*) (55 ± 2%, $p = 0.0042$). In contrast, the effect of ChABC treatment was dramatically enhanced in *Ptprz1* KO cultures and led to a virtually complete loss of aggrecan staining in these cells (Fig. 7*F*) (14 ± 3%, $p = 0.0202$). Further, this effect of ChABC treatment was significantly different between the two genotypes ($p = 0.0015$). EGTA treatment alone only had a small effect on aggrecan staining in both WT (Fig. 7*C*) (79 ± 11%, $p = 0.3788$) and *Ptprz1* KO cultures (Fig. 7*G*) (84 ± 19%, $p = 0.9958$). Interestingly, the combination of the two treatments, *i.e.* ChABC in conjunction with EGTA, led to almost complete loss of aggrecan in WT (Fig. 7*D*) (11 ± 2%, $p <$ 0.0001) as well as *Ptprz1* KO cultures (Fig. 7*H*) (9 ± 2%, $p =$ 0.0137). These findings confirm our previous result and indicate that PNN component aggrecan is immobilized on the cell surface via two interactions, being sensitive to ChABC and a loss of Ca^{2+} ions, respectively. Further they indicate that the Ca^{2+}-dependent interaction is mediated by RPTPζ and is compromised in the *Ptprz1* KO animals.

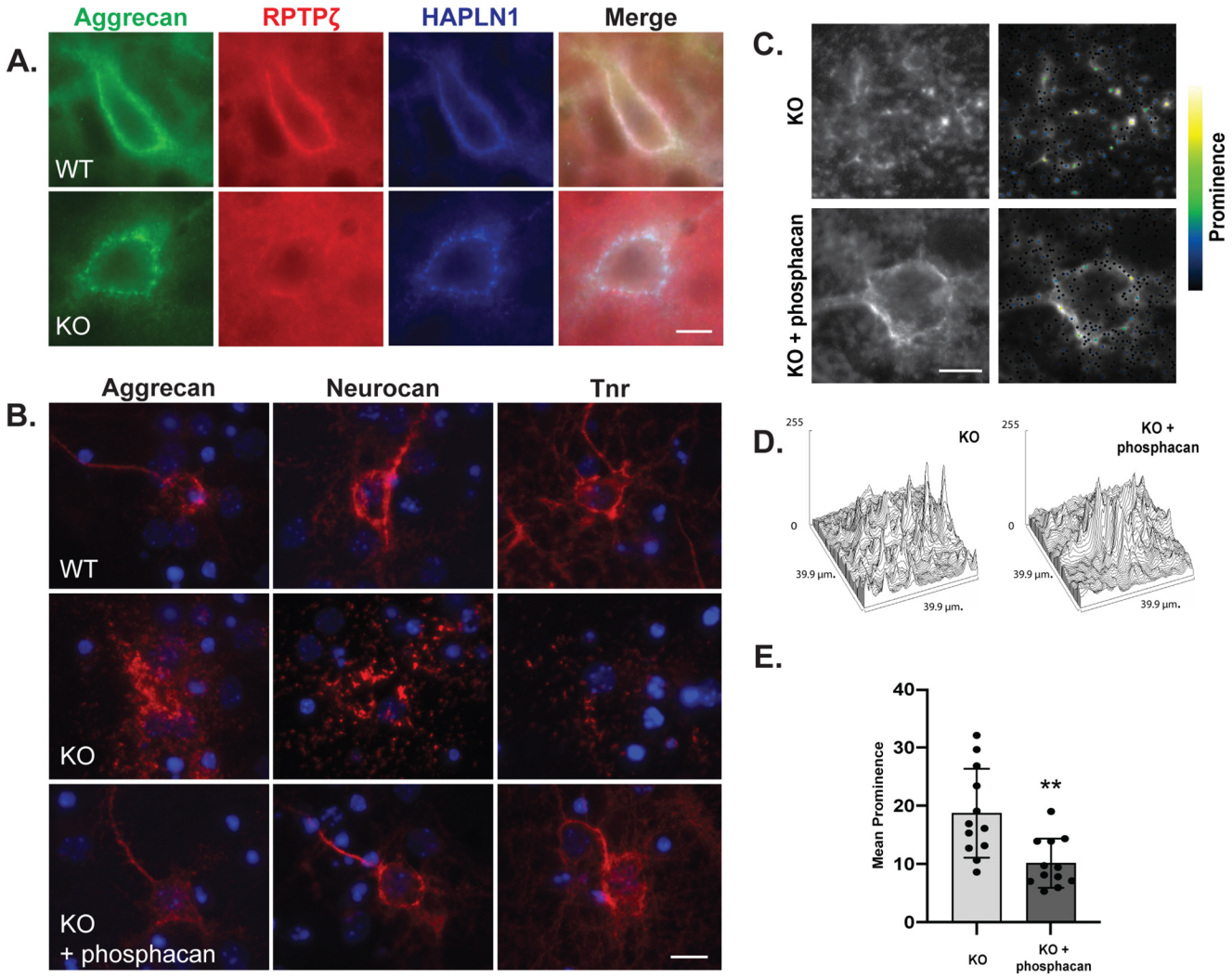

Figure 8. Phosphacan and Tnr cooperate to stabilize PNN components to the neuronal surface. *A*, in PND 90 adult cortical sections from *Tnr* KO mice, RPTPζ (3F8) was largely reduced in PNNs (detected with anti-aggrecan antibodies) compared with WT mice. Of note, HAPLN1 still persists on PNNs in *Tnr* KO mice. Scale bar, 10 μm. *B*, cortical cultures derived from E16 WT and *Ptprz1* KO were fixed at DIV 9 and stained with PNN components, aggrecan, neurocan, and Tnr. We observed a distinct disruption of these components in *Ptprz1* KO neuronal cultures when compared with WT. In addition, Tnr expression is largely reduced in *Ptprz1* KO neuronal cultures. To determine which *Ptprz1* isoform contributes to PNN structure, we purified the soluble form, phosphacan from PND 4 mouse brains through anion exchange chromatography. Purified phosphacan (0.25 μg) was added to *Ptprz1* KO neuronal cultures at 3 DIV. Cells were fixed and stained at 9 DIV for PNN components. Intriguingly, exogenous phosphacan seemingly recovered disrupted ECM to resemble WT morphology and expression, suggesting an unknown phosphacan receptor is important for PNN structure. Combining the above data, we conclude Tnr stabilizes the binding of the soluble isoform phosphacan to an unknown receptor on the neuronal surface. *Scale bar*, 10 μm. We quantified this using PNN node/peak analysis. *C*, representative images of *Ptprz1* KO and *Ptprz1* KO + phosphacan nodes or peaks at varying prominence levels. *Yellow* color dots represent nodes of highest prominence (more isolated) followed by *green*, *blue*, and *black*. *D*, representative surface intensity profile of PNNs. *E*, the average isolation index of PNNs represented by the mean prominence of peaks is significantly less in *Ptprz1* KO + phosphacan PNNs ($n = 12$ PNNs, 3 cultures) compared with *Ptprz1* KO cells ($n = 12$ PNNs, 4 cultures) indicating a decrease in the sharpness of PNN nodes or peaks with phosphacan addition in *Ptprz1* KO neuronal cultures ($p = 0.002$, two-tailed Student's *t* test, S.D. for *error bars*). *Scale bar*, 10 μm.

Phosphacan and tenascin-R cooperate to stabilize PNN components to the neuronal surface

Currently, we have shown that Tnr remains bound to PNNs in *Ptprz1* KO mice. If RPTPζ does indeed anchor PNNs through Tnr, we would expect RPTPζ to remain present on PNNs in *Tnr* KO mice. To test this hypothesis, we stained for RPTPζ on cortical sections of *Tnr* mice (Fig. 8*A*). Intriguingly RPTPζ, although prominent in *Tnr* WT, was greatly diminished on *Tnr* KO PNNs consistent with previous studies (26). This suggests Tnr expression is needed to maintain RPTPζ on the neuronal surface of PNNs. This made us investigate which specific isoform of RPTPζ is required for PNN structure in an effort to better understand the molecular composition of PNNs

To clarify which *Ptprz1* isoform, RPTPζ or phosphacan, serves to anchor PNNs to the neuronal cell surface, we turned to our culture model system. To differentiate between isoforms, we purified soluble phosphacan from P4 mouse brains and exogenously added it to *Ptprz1* WT and KO neuronal cultures. If only the receptor form RPTPζ anchored PNN structures, we would not expect the exogenous addition of phosphacan to have any affect in our PNN culture model system. Phosphacan was added to *Ptprz1* cultures starting at 3 DIV. Cultures were then fixed at 9 DIV and immunostained for PNN components aggrecan, neurocan, and Tnr (Fig. 8*B*).

In *Ptprz1* WT cultures, aggrecan and neurocan tightly coated a population of neuronal cell bodies and proximal neurites,

whereas in *Ptprz1* KO neuronal cultures, aggrecan and neurocan indiscriminately aggregated on neuronal surfaces, losing most discernable cell surface structure. Although Tnr was also spatially disrupted in *Ptprz1* KO cultures, its expression on the neuronal surface was greatly diminished. After phosphacan addition to *Ptprz1* KO cultures, the aggregated aggrecan and neurocan phenotype and reduced expression of Tnr in *Ptprz1* KO cultures remarkably recovered to control conditions. To quantify the recovery of PNN structures in *Ptprz1* KO neurons we utilized aggrecan staining and peak node/analysis as previously described. Addition of phosphacan to *Ptprz1* KO cultures was sufficient to restore the spatial distribution of PNN components on the cell surface making them appear more continuous and less isolated (Fig. 8, *C* and *D*). Further, the average isolation index or mean prominence of PNN peaks was significantly lower in the *Ptprz1* KO cultures with phosphacan addition as compared with *Ptprz1* KO cultures alone ($p = 0.002$, two-tailed Student's t test) (Fig. 8*E*). These data indicate that phosphacan, not RPTPζ, serves as an anchor to maintain proper spatial distribution of ECM components *in vitro* and, therefore, is likely the key *Ptprz1* isoform that maintains the PNN lattice-like structure. Of particular interest, because of the soluble nature of phosphacan, it must bind to an unknown membrane-embedded receptor to anchor PNNs. Considering the above data, we conclude Tnr stabilizes the binding of the soluble form phosphacan to this unknown receptor on the neuronal surface and it is this binding and the interaction between both proteins that is critical for the intricate PNN lattice-like structure.

Discussion

Understanding and defining the molecular composition and structure of PNNs are a critical step toward unlocking their function. In the current study, we demonstrate a novel and unique role for the CSPG RPTPζ in the structure of PNNs. We show that in cooperation with Tnr, RPTPζ provides a key link to the neuronal surface, thereby generating the netlike or lattice-like structure of PNNs. These studies enabled us to create a new model of PNN structural composition that will direct more precise investigation of PNN function.

PNNs were first described over a century ago by Camillo Golgi and even though more than a hundred years of PNN research have passed, their structure and exact molecular composition has remained elusive. These structures form a subcompartment of the neural ECM but are clearly distinct from the surrounding matrix (25, 31). They are highly ordered and stable and demonstrate a unique geometry which is absent in the broader ECM (11, 43, 44). PNNs look like a mesh covering the surface of particular subsets of neurons. This meshlike appearance derives from the fact that PNN components are excluded from points of synaptic contact on the neuronal soma (45). We show here that this ordered distribution of PNNs on the neuronal surface depends on RPTPζ. In particular, there is a specific loss of the reticular structure of PNNs in *Ptprz1* KO animals. Interestingly, most PNN components remain bound to the surface of the appropriate neurons in *Ptprz1* KO animals but they no longer have a netlike structure. This is the first direct demonstration that RPTPζ is critically involved in PNN structure.

We noted that the altered PNNs in *Ptprz1* KO animals brains seemed to significantly phenocopy disruptions previously found in *Tnr* KO mice (26, 37). Our results suggest that these two PNN components are a part of the same binding mechanism immobilizing PNNs and a loss of either leads to disruption and loss of staining of their components. RPTPζ is a known high-affinity ligand for Tnr (29, 30, 46). We therefore sought to better understand the biochemical nature and order of Tnr and RPTPζ binding within PNNs. Our studies here and the work of others (26) show that in Tnr-deficient brains, RPTPζ staining is reduced in PNNs, suggesting Tnr is perhaps responsible for recruiting RPTPζ to PNNs. In contrast, in primary neuronal cultures from RPTPζ knockout brains Tnr is dramatically reduced in netlike structures. Furthermore, in studies in HEK293 cells we found that RPTPζ was necessary to recruit Tnr and other PNN components to the cell surface. Therefore, overall our data suggest a cooperative mechanism by which Tnr and RPTPζ contribute to cell surface binding of PNNs.

It is of particular interest that, even though PNNs are disrupted in mice lacking RPTPζ or Tnr, the total number and distribution of PNNs in the cortex is not obviously changed. One possible explanation for this is that a key component for PNN formation, the glycosaminoglycan HA, is still expressed by these cells and this could be another nucleating molecule for the formation on PNNs. The current structural model of PNNs revolves around the lectican family of CSPGs binding to HA, which acts as backbone for PNN formation. The entire structure of HA and CSPGs is then crosslinked by Tnr. Future studies will evaluate if knocking out both Tnr and RPTPζ leads to a more pronounced phenotype to determine whether they functionally depend on each other. In our biochemical assays, the absence of RPTPζ or Tnr left PNN components susceptible to release by digesting away the HA backbone, in contrast to WT tissue that required disruption of both the HA backbone and Tnr/RPTPζ interaction. Further, the interaction between HA and CSPGs is stabilized by the protein HAPLN1 (47, 48). In mice carrying null alleles for HAPLN1, the interaction between CSPGs and HA is thought to be destabilized. PNNs in these *HAPLN1* KO mice appear attenuated but the disruption is distinct from the structurally deficient PNNs of the *Tnr* KO mice (26, 37, 49, 50).

Our findings along with existing data on PNN structure suggest that PNN components are immobilized on the neuronal surface by two distinct interactions. One dependent on Tnr and RPTPζ being sensitive to Ca^{2+} ions and the other dependent on HAPLN1 and the HA backbone, susceptible to enzymatic digestion of HA. These findings enabled us to create a new and more refined model of PNN structure (Fig. 9). In this model, lectican CSPGs are bound to the HA backbone and stabilized by HAPLN1. These CSPGs are then crosslinked to RPTPζ by Tnr, which acts as an adapter protein between the two arms. Our data suggest that this interaction of the CSPGs with Tnr and RPTPζ is responsible for the meshlike appearance of PNNs and an absence of this interaction leads to the discontinuous and aggregated phenotype of PNNs seen in the *Tnr* KO and *Ptprz1* KO mice. It should be noted that RPTPζ exists in mul-

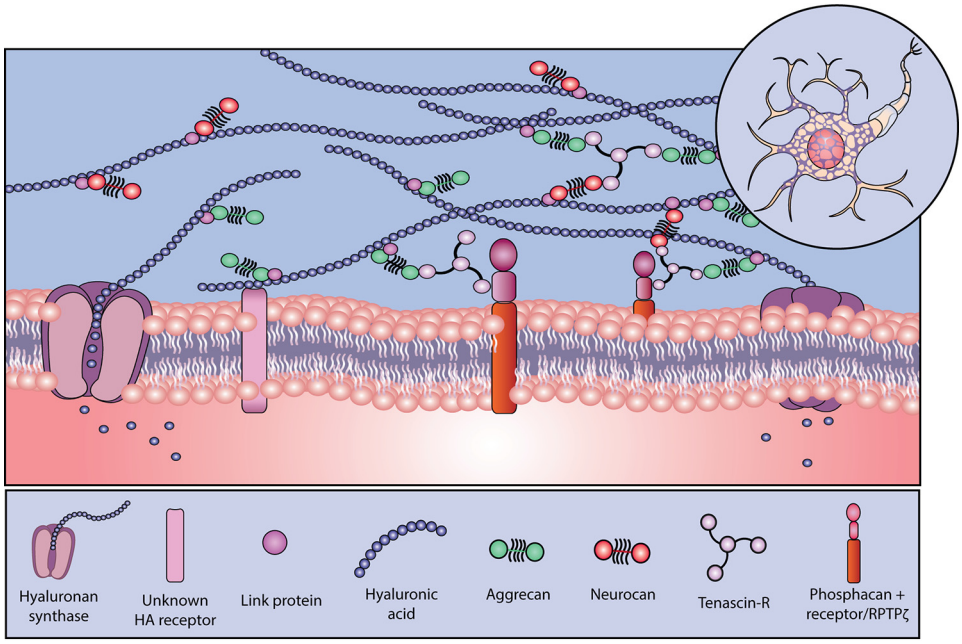

Figure 9. Proposed novel PNN structural model. We propose a two-arm model for PNNs, in which each arm is uniquely attached to the cell surface. On one arm is HA-mediated cell surface binding to an unknown receptor. The other arm depends on the complex between tenascin-R (Tnr) and the secreted *Ptprz1* isoform phosphacan. Our data suggest Tnr and phosphacan stabilize each other to bind to an unknown receptor. In addition, this complex is also dependent on the divalent ion Ca^{2+}.

tiple forms, splice isoforms and proteolytic cleavage products (51–53). We have also shown that PNN component–binding can be partially recovered by adding the soluble form of RPTPζ (phosphacan) to dissociated neurons derived from *Ptprz1* KO mice and these "rescued" neurons showed recovered binding of PNN components to the neuronal cell surface. Our data suggest that phosphacan interacts with Tnr and binds PNNs to the neuronal surface. A question therefore remains for a receptor that binds phosphacan to the neuron. RPTPζ is known to interact with several cell-surface adhesion molecules, including Ng-CAM, N-CAM, and Nr-CAM, as well as other cell surface molecules like contactin (54). It remains to be determined how soluble RPTPζ remains attached to the cell surface, as a goal of future studies. In addition we cannot formally rule out the possibility that the receptor form of RPTPζ plays a role in net structure *in vivo*. In fact humans do not make a secreted form of RPTPζ and therefore further studies will be needed specifically targeting the receptor form to determine its specific role in PNNs. Our work also suggests that a key nucleating event of PNN formation involves cell-surface HA; defining how HA attaches to the neuronal cell surface may provide a further key to understanding PNN specificity and structure (23, 32, 40).

Experimental procedures

Animals

Mice lacking the *Ptprz1* gene (*Ptprz1* KO) were generated as described previously (55) and received from Dr. Sheila Harroch (Department of Neuroscience, Institute Pasteur, Paris, France). Tenascin-R knockout (*Tnr* KO) adult brains (27) used for immunohistochemistry and biochemistry experiments were from Dr. Morawski's laboratory. For neuronal cultures, in addition to *Ptprz1* KO mice, timed pregnant CD-1 WT mice were purchased from Charles River Laboratories (Wilmington, MA). All experiments followed the protocols approved by the Institutional Animal Care and Use Committee of Upstate Medical University.

Antibodies

Mouse anti-phosphacan (3F8) antibody was obtained from the Developmental Studies Hybridoma Bank. Mouse anti–tenascin-R 619, sheep anti-neurocan, and goat anti-HAPLN1 was purchased from R&D Systems (Minneapolis, MN). Rabbit anti-B756, which detects amino acids 420–433 of rat brevican (56). Rabbit anti-aggrecan and mouse β-actin were both purchased from MilliporeSigma (Burlington, MA). Mouse anti-aggrecan was purchased from Bio-Rad Laboratories. Fluorescein labeled WFA was purchased from Vector Laboratories (Burlingame, CA).

Preparation of homogenates and soluble and insoluble fractions

Brain homogenates for the aggrecan release assays were derived from postnatal day 90 (PND 90) *Ptprz1* WTs and *Ptprz1* KOs. Tissue was homogenized in 150 mM sodium chloride and 50 mM Tris with EDTA-free protease inhibitor tablets (Roche, 1 tablet in 10 ml buffer) in a Potter-Elvehjem homogenizer. Homogenates were centrifuged at 8000 × *g* for 10 min at 4 °C. The supernatant was then removed, the pellet washed once and then resuspended in 1 ml buffer. A Bradford (Bio-Rad) assay was performed and protein concentrations were adjusted to 2.5 mg/ml. Samples were treated with 2 μl chondroitinase ABC (Sigma-Aldrich) per 500 μl of sample and/or 1 mM EDTA for 8 h. Samples were centrifuged again at 8000 × *g* for 10 min to separate soluble released fraction from insoluble pellet and prepared for Western blotting.

For analysis of overall expression of ECM components by Western blotting, PND 90 brains were homogenized in 5 volumes of 25 mM Tris (pH 7.4) containing protease inhibitor mixture, EDTA-free, and processed for analysis.

Primary cortical cultures

Neuronal primary cultures were prepared as described previously (23). Briefly, cortices of embryonic day (E) 16 CD-1 WT or *Ptprz1* KO embryos were removed and digested in 0.25% trypsin-EDTA (Thermo Fisher Scientific). Mixed cells were filtered and suspended in Neurobasal medium with 3% B27, 1× GlutaMAX and 1× penicillin-streptomycin (Thermo Fisher Scientific). Cells were then plated at a density of 2.1×10^6 on coverslips (500 μl/per well) precoated with poly-D-lysine (50 μg/ml) and laminin (5 μg/ml) (Sigma-Aldrich) in a 24-well dish. To remove glia, cells were treated with 5 μM cytosine arabinoside (AraC, Sigma-Aldrich) at 1 day *in vitro* (DIV). The medium was then changed at 3 DIV to remove AraC, and given a half change at 6 DIV. Cells were maintained at 37 °C 5% CO_2 until fixation.

Phosphacan was purified by anion exchange chromatography as described previously (57). Briefly, the soluble fraction, from PND 4 CD-1 mouse brain, was filtered using a PVDF 0.22 μM filter, brought to a 0.5 M NaCl concentration, and run through a 1 ml HiTrap-Q HP column using a peristaltic pump connected to an Amersham Biosciences Pharmacia RediFrac fraction collector (GE Healthcare Life Sciences). Sample was eluted over a continuous gradient of 0.5 M NaCl to 2.0 M NaCl over 10 column volumes and collected as 250 μl fractions. Phosphacan-rich fractions, identified by dot blot analysis, were pooled and concentrated using 100,000 MWCO Concentrators (AmiconUltra, EMD Millipore). Approximately 250 ng of purified phosphacan was added to *Ptprz1* KO cultures after the first medium change at 3 DIV and 125 ng was added after the half-medium change at 6 DIV and analyzed at 9 DIV. When noted, coverslips were treated with 10 μl ChABC for 30 min and/or 2.5 mM EGTA for 15 min. Coverslips were fixed and subsequently processed for immunocytochemistry.

Immunocytochemistry and immunohistochemistry

Primary cortical cultures plated on coverslips were fixed at 9 DIV in cold 4% phosphate-buffered paraformaldehyde (PFA) with 0.01% glutaraldehyde, pH 7.4. Cells were then blocked in screening medium (DMEM, 5% FBS, 0.2% sodium azide) for 1 h, before adding primary antibodies overnight at 4 °C. The following day, Alexa Fluor–conjugated secondary antibodies (Thermo Fisher Scientific) in screening medium were added to the cells for 2 h before mounting the coverslips with ProLong Antifade Kit (Thermo Fisher Scientific). Cell nuclei were visualized with Hoechst solution (Thermo Fisher Scientific) diluted in 1× PBS. For immunohistochemistry on tissue sections, PND 90 *Ptprz1* and *Tnr* (all genotypes) mice were transcardially perfused with cold PBS (Thermo Fisher Scientific) prior to fixation with 4% PFA. Brains were postfixed overnight in 4% PFA before changing to a 30% sucrose solution diluted in phosphate buffer with 0.2% sodium azide. Using a cryostat, brains were cut as free-floating sections at 40 μM and placed in phosphate buffer with 0.2% sodium azide. Sections were blocked 1 h at room temperature and then stained in either 5% milk in TBST with 1% Triton X-100 (mouse anti-tenascin-R 619, sheep anti-neurocan, rabbit anti-brevican) or screening medium with 1% Triton X-100 (WFA, mouse anti-aggrecan, goat anti-HAPLN1, and mouse anti-phosphacan). Tissue sections were additionally stained with Hoechst solution to visualize nuclei before being mounted on glass slides. Both cells and tissue were imaged using an epi-fluorescent Zeiss Imager.A2 with Nikon Elements software package. Final images were gathered and formatted using ImageJ software (58) and assembled into figures using Adobe Illustrator CC 2019.

SDS-PAGE and Western blotting

Protein concentrations were determined by Bradford assay before gel electrophoresis. For detection of CSPGs, brain lysates were treated with 2 μl ChABC (Millipore Sigma, C3667, 0.1mU/μl) for 8 h at 37 °C to remove chondroitinase sulfate side chains and allow proper gel migration. SDS-polyacrylamide gels, used at either 4–12% or 6–15% gradient, were transferred to 0.45 μM nitrocellulose membranes. Western blotting was conducted as described previously (59). Briefly, blots were placed in blocking buffer composed of 5% milk in low-salt TBST and then incubated in primary antibody overnight. Blots were then incubated in HRP-conjugated secondary antibodies (The Jackson Laboratory, Bar Harbor, ME) and exposed using SuperSignal West Pico Chemiluminescent Substrate or SuperSignal West Femto Chemiluminescent Substrate (Thermo Fisher Scientific). Blots were imaged using ChemiDoc MP system (Bio-Rad) or using Premium X-ray film (Phenix Research Products, Candler, NC).

Quantification and statistical analyses

The binary gap analysis was used to quantify regions devoid of PNN. For analysis, high magnification z-stack images (0.25 μM steps, 63× magnification) of PNNs, visualized with WFA, were taken throughout the PND 90 adult somatosensory cortex (Bregma, −2.46 mm) of *Ptprz1* strain mice. To better visualize PNN surface structure, nets were flattened using the Z-project, max intensity function on ImageJ (58). Once flattened, a fixed region excluding the PNN periphery (~25 μm^2) was cropped from the estimated center of the PNN and thresholded to obtain a binary (black and white) image to analyze the PNN surface. The black/white pixel count ratio for each PNN was determined using the histogram function and averaged for each genotype.

PNN peak or node analysis was used to quantitatively describe the PNN aggregation seen on the surface of neurons in *Tnr* KO and *Ptprz1* KO mice. Z-projected images of the PNN were processed using the local maxima function of ImageJ to identify peaks (nodes) of intense PNN staining. Once the nodes were identified, an ad hoc algorithm was used to measure the average distance between those nodes and the difference in intensity between the nodes and their surrounding space on the cell surface (node prominence) The number of unique nodes and their mean prominence was plotted for each genotype.

The quantification of ECM components in *Ptprz1* KO was assessed through immunohistochemistry (IHC) and Western blot analysis. For IHC, adult coronal sections approximately at Bregma −2.46 mm were stained to detect the PNN-specific

components aggrecan, WFA (detects CS chains, dependent on aggrecan expression) and HAPLN1, and the PNN-associated components brevican, neurocan, and tenascin-R (Tnr). For quantification of specific net components, 10× large stitch images, processed by the Nikon Elements software, were taken of the cortex of *Ptprz1* KO and WT mice. The pixel intensity of each specific PNN component was determined by taking a region of interest of the cortex and using the measure function of ImageJ. To quantify nonspecific PNN markers (brevican, neurocan, and Tnr), a region of interest and intensity measurement was taken of a sample set of individual PNNs (average of 25 PNNs per animal) throughout the adult cortices (images taken at 20×). PNN pixel intensity was then averaged for each genotype and significance determined using an unpaired Student's t test, $p < 0.05$. To produce bar graphs, data were normalized and scaled.

Western blot analysis was used to further quantify the PNN-specific components aggrecan and HAPLN1. Cortices were specifically taken from *Ptprz1* KO and WT mice, homogenized, separated on a 4–12% SDS-polyacrylamide gel and transferred to nitrocellulose for blotting. Western blots for aggrecan and HAPLN1 expression were imaged using ChemiDoc MP system (Bio-Rad) and analyzed in ImageJ. Expression was determined by taking the average ratio of PNN-specific component intensity to β-actin intensity for each genotype. Differences were found significant at $p < 0.05$ (unpaired Student's t test or analysis of variance (ANOVA) with Tukey's post hoc analyses as appropriate) using GraphPad Prism 7/8 or RStudio statistical software.

Author contributions—G. J. E. and A. S. data curation; G. J. E., A. S., M. S. V., and R. T. M. formal analysis; G. J. E., A. S., and R. T. M. investigation; G. J. E. and A. S. visualization; G. J. E., A. S., and M. S. V. methodology; G. J. E. and A. S. writing-original draft; M. M., M. S. V., and R. T. M. conceptualization; M. M. and R. T. M. resources; M. M. and R. T. M. funding acquisition; M. M., M. S. V., and R. T. M. writing-review and editing; R. T. M. supervision; R. T. M. project administration.

Acknowledgment—We thank Dr. Mandy Sonntag for helping with preparation of the tissue from the tenascin-R knockout mice.

References

1. Pizzorusso, T., Medini, P., Berardi, N., Chierzi, S., Fawcett, J. W., and Maffei, L. (2002) Reactivation of ocular dominance plasticity in the adult visual cortex. *Science* **298,** 1248–1251 CrossRef Medline
2. Gogolla, N., Caroni, P., Lüthi, A., and Herry, C. (2009) Perineuronal nets protect fear memories from erasure. *Science* **325,** 1258–1261 CrossRef Medline
3. Romberg, C., Yang, S., Melani, R., Andrews, M. R., Horner, A. E., Spillantini, M. G., Bussey, T. J., Fawcett, J. W., Pizzorusso, T., and Saksida, L. M. (2013) Depletion of perineuronal nets enhances recognition memory and long-term depression in the perirhinal cortex. *J. Neurosci.* **33,** 7057–7065 CrossRef Medline
4. Yang, S., Cacquevel, M., Saksida, L. M., Bussey, T. J., Schneider, B. L., Aebischer, P., Melani, R., Pizzorusso, T., Fawcett, J. W., and Spillantini, M. G. (2015) Perineuronal net digestion with chondroitinase restores memory in mice with tau pathology. *Exp. Neurol.* **265,** 48–58 CrossRef Medline
5. Pantazopoulos, H., Woo, T.-U. W., Lim, M. P., Lange, N., and Berretta, S. (2010) Extracellular matrix-glial abnormalities in the amygdala and entorhinal cortex of subjects diagnosed with schizophrenia. *Arch. Gen. Psychiatry.* **67,** 155–166 CrossRef Medline
6. Pantazopoulos, H., Markota, M., Jaquet, F., Ghosh, D., Wallin, A., Santos, A., Caterson, B., and Berretta, S. (2015) Aggrecan and chondroitin-6-sulfate abnormalities in schizophrenia and bipolar disorder: A postmortem study on the amygdala. *Transl. Psychiatry* **5,** e496 CrossRef Medline
7. Mauney, S. A., Athanas, K. M., Pantazopoulos, H., Shaskan, N., Passeri, E., Berretta, S., and Woo, T.-U. W. (2013) Developmental pattern of perineuronal nets in the human prefrontal cortex and their deficit in schizophrenia. *Biol. Psychiatry.* **74,** 427–435 CrossRef Medline
8. Viapiano, M. S., and Matthews, R. T. (2006) From barriers to bridges: Chondroitin sulfate proteoglycans in neuropathology. *Trends Mol. Med.* **12,** 488–496 CrossRef Medline
9. Brückner, G., Brauer, K., Härtig, W., Wolff, J. R., Rickmann, M. J., Derouiche, A., Delpech, B., Girard, N., Oertel, W. H., and Reichenbach, A. (1993) Perineuronal nets provide a polyanionic, glia-associated form of microenvironment around certain neurons in many parts of the rat brain. *Glia* **8,** 183–200 CrossRef Medline
10. Celio, M. R., Spreafico, R., De Biasi, S., and Vitellaro-Zuccarello, L. (1998) Perineuronal nets: Past and present. *Trends Neurosci.* **21,** 510–515 CrossRef Medline
11. Lander, C., Kind, P., Maleski, M., and Hockfield, S. (1997) A family of activity-dependent neuronal cell-surface chondroitin sulfate proteoglycans in cat visual cortex. *J. Neurosci.* **17,** 1928–1939 CrossRef Medline
12. Hockfield, S., Kalb, R. G., Zaremba, S., and Fryer, H. (1990) Expression of neural proteoglycans correlates with the acquisition of mature neuronal properties in the mammalian brain. in *Cold Spring Harb. Symp. Quant. Biol.* **55,** 505–514 CrossRef Medline
13. McKeon, R. J., Schreiber, R. C., Rudge, J. S., and Silver, J. (1991) Reduction of neurite outgrowth in a model of glial scarring following CNS injury is correlated with the expression of inhibitory molecules on reactive astrocytes. *J. Neurosci.* **11,** 3398–3411 CrossRef Medline
14. Niederöst, B. P., Zimmermann, D. R., Schwab, M. E., and Bandtlow, C. E. (1999) Bovine CNS myelin contains neurite growth-inhibitory activity associated with chondroitin sulfate proteoglycans. *J. Neurosci.* **19,** 8979-8989 CrossRef Medline
15. Bradbury, E. J., Moon, L. D., Popat, R. J., King, V. R., Bennett, G. S., Patel, P. N., Fawcett, J. W., and McMahon, S. B. (2002) Chondroitinase ABC promotes functional recovery after spinal cord injury. *Nature* **416,** 636–640 CrossRef Medline
16. McRae, P. A., Rocco, M. M., Kelly, G., Brumberg, J. C., and Matthews, R. T. (2007) Sensory deprivation alters aggrecan and perineuronal net expression in the mouse barrel cortex. *J. Neurosci.* **27,** 5405–5413 CrossRef Medline
17. Balmer, T. S., Carels, V. M., Frisch, J. L., and Nick, T. A. (2009) Modulation of perineuronal nets and parvalbumin with developmental song learning. *J. Neurosci.* **29,** 12878–12885 CrossRef Medline
18. Pizzorusso, T., Medini, P., Landi, S., Baldini, S., Berardi, N., and Maffei, L. (2006) Structural and functional recovery from early monocular deprivation in adult rats. *Proc. Natl. Acad. Sci. U.S.A.* **103,** 8517–8522 CrossRef Medline
19. Xue, Y.-X., Xue, L.-F., Liu, J.-F., He, J., Deng, J.-H., Sun, S.-C., Han, H.-B., Luo, Y.-X., Xu, L.-Z., Wu, P., and Lu, L. (2014) Depletion of perineuronal nets in the amygdala to enhance the erasure of drug memories. *J. Neurosci.* **34,** 6647–6658 CrossRef Medline
20. Végh, M. J., Heldring, C. M., Kamphuis, W., Hijazi, S., Timmerman, A. J., Li, K. W., van Nierop, P., Mansvelder, H. D., Hol, E. M., Smit, A. B., and van Kesteren, R. E. (2014) Reducing hippocampal extracellular matrix reverses early memory deficits in a mouse model of Alzheimer's disease. *Acta Neuropathol. Commun.* **2,** 76 CrossRef Medline
21. Slaker, M., Churchill, L., Todd, R. P., Blacktop, J. M., Zuloaga, D. G., Raber, J., Darling, R. A., Brown, T. E., and Sorg, B. A. (2015) Removal of perineuronal nets in the medial prefrontal cortex impairs the acquisition and reconsolidation of a cocaine-induced conditioned place preference memory. *J. Neurosci.* **35,** 4190–4202 CrossRef Medline
22. Lee, H., Leamey, C. A., and Sawatari, A. (2012) Perineuronal nets play a role in regulating striatal function in the mouse. *PLoS One* **7,** e32747 CrossRef Medline

23. Giamanco, K. A., Morawski, M., and Matthews, R. T. (2010) Perineuronal net formation and structure in aggrecan knockout mice. *Neuroscience* **170,** 1314–1327 CrossRef Medline
24. Rowlands, D., Lensjø, K. K., Dinh, T., Yang, S., Andrews, M. R., Hafting, T., Fyhn, M., Fawcett, J. W., and Dick, G. (2018) Aggrecan directs extracellular matrix-mediated neuronal plasticity. *J. Neurosci.* **38,** 10102–10113 CrossRef Medline
25. Deepa, S. S., Carulli, D., Galtrey, C., Rhodes, K., Fukuda, J., Mikami, T., Sugahara, K., and Fawcett, J. W. (2006) Composition of perineuronal net extracellular matrix in rat brain: A different disaccharide composition for the net-associated proteoglycans. *J. Biol. Chem.* **281,** 17789–17800 CrossRef Medline
26. Brückner, G., Grosche, J., Schmidt, S., Härtig, W., Margolis, R. U., Delpech, B., Seidenbecher, C. I., Czaniera, R., and Schachner, M. (2000) Postnatal development of perineuronal nets in wild-type mice and in a mutant deficient in tenascin-R. *J. Comp. Neurol.* **428,** 616–629 CrossRef Medline
27. Weber, P., Bartsch, U., Rasband, M. N., Czaniera, R., Lang, Y., Bluethmann, H., Margolis, R. U., Levinson, S. R., Shrager, P., Montag, D., and Schachner, M. (1999) Mice deficient for tenascin-R display alterations of the extracellular matrix and decreased axonal conduction velocities in the CNS. *J. Neurosci.* **19,** 4245–4262 CrossRef Medline
28. Barnea, G., Grumet, M., Milev, P., Silvennoinen, O., Levy, J. B., Sap, J., and Schlessinger, J. (1994) Receptor tyrosine phosphatase beta is expressed in the form of proteoglycan and binds to the extracellular matrix protein tenascin. *J. Biol. Chem.* **269,** 14349–14352 Medline
29. Xiao, Z., Bartsch, U., Margolis, K., Montag, D., Schachner, M., and Zu, C. (1997) Isolation of a tenascin-R binding protein from mouse brain membranes. A phosphacan-related chondroitin sulfate proteoglycan. *J. Biol. Chem.* **272,** 32092–32101 CrossRef Medline
30. Milev, P., Chiba, A., Häring, M., Rauvala, H., Schachner, M., Ranscht, B., Margolis, R. K., and Margolis, R. U. (1998) High affinity binding and overlapping localization of neurocan and phosphacan protein-tyrosine phosphatase-zeta/beta with tenascin-R, amphoterin, and the heparin-binding growth-associated molecule. *J. Biol. Chem.* **273,** 6998–7005 CrossRef Medline
31. Grumet, M., Milev, P., Sakurai, T., Karthikeyan, L., Bourdon, M., Margolis, R. K., and Margolis, R. U. (1994) Interactions with tenascin and differential effects on cell adhesion of neurocan and phosphacan, two major chondroitin sulfate proteoglycans of nervous tissue. *J. Biol. Chem.* **269,** 12142–12146 Medline
32. Haunsø, A., Ibrahim, M., Bartsch, U., Letiembre, M., Celio, M. R., and Menoud, P. (2000) Morphology of perineuronal nets in tenascin-R and parvalbumin single and double knockout mice. *Brain Res.* **864,** 142–145 CrossRef Medline
33. Morawski, M., Dityatev, A., Hartlage-Ruebsamen, M., Blosa, M., Holzer, M., Flach, K., Pavlica, S., Dityateva, G., Grosche, J., Brueckner, G., and Schachner, M. (2014) Tenascin-R promotes assembly of the extracellular matrix of perineuronal nets via clustering of aggrecan. *Philos. Trans. R. Soc. Lond. B Biol. Sci.* **369,** 20140046 CrossRef Medline
34. Carulli, D., Rhodes, K. E., Brown, D. J., Bonnert, T. P., Pollack, S. J., Oliver, K., Strata, P., and Fawcett, J. W. (2006) Composition of perineuronal nets in the adult rat cerebellum and the cellular origin of their components. *J. Comp. Neurol.* **494,** 559–577 CrossRef Medline
35. Kwok, J. C. F., Carulli, D., and Fawcett, J. W. (2010) *In vitro* modeling of perineuronal nets: Hyaluronan synthase and link protein are necessary for their formation and integrity. *J. Neurochem.* **114,** 1447–1459 CrossRef Medline
36. John, N., Krügel, H., Frischknecht, R., Smalla, K. H., Schultz, C., Kreutz, M. R., Gundelfinger, E. D., and Seidenbecher, C. I. (2006) Brevican-containing perineuronal nets of extracellular matrix in dissociated hippocampal primary cultures. *Mol. Cell Neurosci.* **31,** 774–784 CrossRef Medline
37. Matthews, R. T., Kelly, G. M., Zerillo, C. A., Gray, G., Tiemeyer, M., and Hockfield, S. (2002) Aggrecan glycoforms contribute to the molecular heterogeneity of perineuronal nets. *J. Neurosci.* **22,** 7536–7547 CrossRef Medline
38. Giamanco, K. A., and Matthews, R. T. (2012) Deconstructing the perineuronal net: Cellular contributions and molecular composition of the neuronal extracellular matrix. *Neuroscience* **218,** 367–384 CrossRef Medline
39. Zhou, X. H., Brakebusch, C., Matthies, H., Oohashi, T., Hirsch, E., Moser, M., Krug, M., Seidenbecher, C. I., Boeckers, T. M., Rauch, U., Buettner, R., Gundelfinger, E. D., and Fässler, R. (2001) Neurocan is dispensable for brain development. *Mol. Cell Biol.* **21,** 5970–5978 CrossRef Medline .
40. Brakebusch, C., Seidenbecher, C. I., Asztely, F., Rauch, U., Matthies, H., Meyer, H., Krug, M., Bo, T. M., Zhou, X., Kreutz, M. R., Montag, D., Gundelfinger, E. D., and Fa, R. (2002) Brevican-deficient mice display impaired hippocampal CA1 long-term potentiation but show no obvious deficits in learning and memory. *Mol. Cell. Biol.* **22,** 7417–7427 CrossRef Medline
41. Suttkus, A., Rohn, S., Weigel, S., Glöckner, P., Arendt, T., and Morawski, M. (2014) Aggrecan, link protein and tenascin-R are essential components of the perineuronal net to protect neurons against iron-induced oxidative stress. *Cell Death Dis.* **5,** e1119 CrossRef Medline
42. Morawski, M., and Sonntag, M. (2018) Perineuronal nets in the superior olivary complex: Development, function, and plasticity. in *The Oxford Handbook of the Auditory Brainstem* (Kandler, K., ed), pp. 1–28, Oxford University Press, New York, New York CrossRef
43. Härtig, W., Derouiche, A., Welt, K., Brauer, K., Grosche, J., Mäder, M., Reichenbach, A., and Brückner, G. (1999) Cortical neurons immunoreactive for the potassium channel Kv3.1b subunit are predominantly surrounded by perineuronal nets presumed as a buffering system for cations. *Brain Res.* **842,** 15–29 CrossRef Medline
44. Arnst, N., Kuznetsova, S., Lipachev, N., Shaikhutdinov, N., Melnikova, A., Mavlikeev, M., Uvarov, P., Baltina, T. V., Rauvala, H., Osin, Y. N., Kiyasov, A. P., and Paveliev, M. (2016) Spatial patterns and cell surface clusters in perineuronal nets. *Brain Res.* **1648,** 214–223 CrossRef Medline
45. Hockfield, S., and McKay, R. D. (1983) A surface antigen expressed by a subset of neurons in the vertebrate central nervous system. *Proc. Natl. Acad. Sci. U.S.A.* **80,** 5758–5761 CrossRef Medline
46. Peles, E., Schlessinger, J., and Grumet, M. (1998) Multi-ligand interactions with receptor-like protein tyrosine phosphatase β: Implications for intercellular signaling. *Trends Biochem. Sci.* **23,** 121–124 CrossRef Medline
47. Tsifrina, E., Ananyeva, N. M., Hastings, G., and Liau, G. (1999) Identification and characterization of three cDNAs that encode putative novel hyaluronan-binding proteins, including an endothelial cell-specific hyaluronan receptor. *Am. J. Pathol.* **155,** 1625–1633 CrossRef Medline
48. Monslow, J., Williams, J. D., Norton, N., Guy, C. A., Price, I. K., Coleman, S. L., Williams, N. M., Buckland, P. R., Spicer, A. P., Topley, N., Davies, M., and Bowen, T. (2003) The human hyaluronan synthase genes: Genomic structures, proximal promoters and polymorphic microsatellite markers. *Int. J. Biochem. Cell Biol.* **35,** 1272–1283 CrossRef Medline
49. Bekku, Y., Su, W., Hirakawa, S., Fa, R., Ohtsuka, A., Kang, J. S., Sanders, J., Murakami, T., Ninomiya, Y., and Oohashi, T. (2003) Molecular cloning of Bral2, a novel brain-specific link protein, and immunohistochemical colocalization with brevican in perineuronal nets. *Mol. Cell Neurosci.* **24,** 148–159 CrossRef Medline
50. Carulli, D., Pizzorusso, T., Kwok, J. C. F., Putignano, E., Poli, A., Forostyak, S., Andrews, M. R., Deepa, S. S., Glant, T. T., and Fawcett, J. W. (2010) Animals lacking link protein have attenuated perineuronal nets and persistent plasticity. *Brain* **133,** 2331–2347 CrossRef Medline
51. Garwood, J., Schnädelbach, O., Clement, A., Schütte, K., Bach, A., and Faissner, A. (1999) DSD-1-proteoglycan is the mouse homolog of phosphacan and displays opposing effects on neurite outgrowth dependent on neuronal lineage. *J. Neurosci.* **19,** 3888–3899 CrossRef Medline
52. Garwood, J., Heck, N., Reichardt, F., and Faissner, A. (2003) Phosphacan short isoform, a novel non-proteoglycan variant of phosphacan/receptor protein tyrosine phosphatase-β, interacts with neuronal receptors and promotes neurite outgrowth. *J. Biol. Chem.* **278,** 24164–24173 CrossRef Medline
53. Chow, J. P. H., Fujikawa, A., Shimizu, H., Suzuki, R., and Noda, M. (2008) Metalloproteinase- and γ-secretase-mediated cleavage of protein-tyrosine phosphatase receptor type Z. *J. Biol. Chem.* **283,** 30879–30889 CrossRef Medline

54. Lamprianou, S., Chatzopoulou, E., Thomas, J.-L., Bouyain, S., and Harroch, S. (2011) A complex between contactin-1 and the protein tyrosine phosphatase PTPRZ controls the development of oligodendrocyte precursor cells. *Proc. Natl. Acad. Sci. U.S.A.* **108,** 17498–17503 CrossRef Medline
55. Harroch, S., Palmeri, M., Rosenbluth, J., Custer, A., Okigaki, M., Shrager, P., Blum, M., Buxbaum, J. D., and Schlessinger, J. (2000) No obvious abnormality in mice deficient in receptor protein tyrosine phosphatase β. *Mol. Cell Biol.* **20,** 7706–7715 CrossRef Medline
56. Blosa, M., Bursch, C., Weigel, S., Holzer, M., Jäger, C., Janke, C., Matthews, R. T., Arendt, T., and Morawski, M. (2016) Reorganization of synaptic connections and perineuronal nets in the deep cerebellar nuclei of Purkinje cell degeneration mutant mice. *Neural Plast.* **2016,** 2828536 CrossRef Medline
57. Dwyer, C. A., Katoh, T., Tiemeyer, M., and Matthews, R. T. (2015) Neurons and glia modify receptor protein-tyrosine phosphatase ζ (RPTPζ)/phosphacan with cell-specific *O*-mannosyl glycans in the developing brain. *J. Biol. Chem.* **290,** 10256–10273 CrossRef Medline
58. Schindelin, J., Arganda-Carreras, I., Frise, E., Kaynig, V., Longair, M., Pietzsch, T., Preibisch, S., Rueden, C., Saalfeld, S., Schmid, B., Tinevez, J.-Y., White, D. J., Hartenstein, V., Eliceiri, K., Tomancak, P., and Cardona, A. (2012) Fiji: An open-source platform for biological-image analysis. *Nat. Methods* **9,** 676–682 CrossRef Medline
59. Viapiano, M. S., Matthews, R. T., and Hockfield, S. (2003) A novel membrane-associated glycovariant of BEHAB/brevican is up-regulated during rat brain development and in a rat model of invasive glioma. *J. Biol. Chem.* **278,** 33239–33247 CrossRef Medline